# Manipulating the Quantum State of an Electrical Circuit

D. Vion *et al.*

*Science* **296**, 886 (2002);
DOI: 10.1126/science.1069372



*Science* (print ISSN 0036-8075; online ISSN 1095-9203) is published weekly, except the last week in December, by the American Association for the Advancement of Science, 1200 New York Avenue NW, Washington, DC 20005. 

to ~150 GPa, consistent with the modulus values of large SWNT bundles (*22*). Although an individual SWNT has an elastic modulus of ~1 TPa, the value can decrease to ~100 GPa for nanotube bundles, owing to the internanotube defects (for example, imperfect lattice of nanotube bundles owing to different nanotube diameters) present along the bundles.

The long nanotube strands created by our direct synthesis technique are an alternative to the fibers and filaments spun from nanotube slurries (*4*). The mechanical and electrical properties of these strands are superior to the latter fibers: The strands can be produced in high yield and continuously, and the thickness of the strands and their length may be further optimized by tuning the processing conditions to produce practically useful nanotube-based macroscale cables.

**References and Notes**


1. S. Iijima, *Nature* **354**, 56 (1991).
2. Z. Pan *et al.*, *Nature* **394**, 631 (1998).
3. H. M. Cheng *et al.*, *Chem. Phys. Lett.* **289**, 602 (1998).
4. B. Vigolo *et al.*, *Science* **290**, 1331 (2000).
5. L. J. Ci *et al.*, *Carbon* **38**, 1933 (2000).
6. M. Endo *et al.*, *J. Phys. Chem. Solids* **54**, 1841 (1993).
7. R. Andrews *et al.*, *Chem. Phys. Lett.* **303**, 467 (1999).
8. H. M. Cheng *et al.*, *Appl. Phys. Lett.* **72**, 3282 (1998).
9. Thiophene and ferrocene were dissolved in the carbon source (liquid *n*-hexane), sprayed into the hydrogen stream, and fed from the top of a vertical heated furnace. The hydrogen flow rate was then adjusted to provide the optimum conditions for nanotube strand formation. The gas flow carried the strands downstream, and the nanotube strands were collected at the bottom of the furnace.
10. A. Thess *et al.*, *Science* **273**, 483 (1996).
11. P. Launois *et al.*, *J. Nanosci. Nanotechnol.* **1**, 125 (2001).
12. Our data correspond to the larger tube numbers in the bundle ($N = 37$; $N = 91$), as displayed in figure 4 of S. Rols, R. Almairac, L. Henrard, E. Anglaret, J. L. Sauvajol [*Eur. Phys. J. B* **10**, 263 (1999)].
13. J. E. Fischer *et al.*, *Phys. Rev. B* **55**, R4921 (1997).
14. P. H. Zhang, P. E. Lammert, V. H. Crespi, *Phys. Rev. Lett.* **81**, 5346 (1998).
15. The true strain $\varepsilon_T$ is defined as $\varepsilon_T = \ln(L_f/L_0)$, where $L_f$ is the real length of the sample and $L_0$ is the original length of the sample. The true strain could also be described as $\varepsilon_T = 2\ln(D_0/D_f)$, assuming that the sample volume is constant, where $D_0$ and $D_f$ are the original diameter and the real diameter of the sample during the measurement, respectively. Therefore, the true stress can be described as $\sigma_T = P/A = 4P\exp(\varepsilon_T)/\pi D_0^2$, where $P$ is the load and $A$ is the real surface area supporting the load. Because $\ln(1+\varepsilon) \approx \varepsilon$ when $\varepsilon < 0.1$, the true stress versus true strain curve has almost the same slope as that of the load versus engineering strain curve in the elastic strain regime.
16. R. H. Baughman *et al.*, *Science* **284**, 1340 (1999).
17. M. M. J. Treacy, T. W. Ebbesen, J. M. Gibson, *Nature* **381**, 678 (1996).
18. E. W. Wong, P. E. Sheehan, C. M. Lieber, *Science* **277**, 1971 (1997).
19. M. F. Yu, B. S. Files, S. Arepalli, R. S. Ruoff, *Phys. Rev. Lett.* **84**, 5552 (2000).
20. J. P. Lu, *Phys. Rev. Lett.* **79**, 1297 (1997).
21. F. Li, H. M. Cheng, S. Bai, G. Gu, M. S. Dresselhaus, *Appl. Phys. Lett.* **77**, 3161 (2000).
22. L. Forró, C. Schönenberger, in *Carbon Nanotubes: Synthesis, Structure, Properties and Applications*, M. S. Dresselhaus, G. Dresselhaus, Ph. Avouris, Eds. (Springer, New York, 2001), pp. 329–390.


23. H.W.Z., C.L.X., and D.H.W. acknowledge financial support from the State Key Project for Fundamental Research of the Ministry of Science and Technology, China, under grant G20000264-04. P.M.A. acknowledges financial support from the NSF through a CAREER grant. B.Q.W. acknowledges support from the NSF Nanoscale Science and Engineering Center, at Rensselaer Polytechnic Institute, for the directed assembly of nanostructures. We also acknowledge useful discussions with N. Koratkar and technical assistance from D. Vansteele and Y. Choi.

10 October 2001; accepted 22 March 2002


# Manipulating the Quantum State of an Electrical Circuit


**D. Vion,* A. Aassime, A. Cottet, P. Joyez, H. Pothier, C. Urbina,† D. Esteve, M. H. Devoret‡**



**We have designed and operated a superconducting tunnel junction circuit that behaves as a two-level atom: the "quantronium." An arbitrary evolution of its quantum state can be programmed with a series of microwave pulses, and a projective measurement of the state can be performed by a pulsed readout subcircuit. The measured quality factor of quantum coherence $Q_\varphi \cong 25{,}000$ is sufficiently high that a solid-state quantum processor based on this type of circuit can be envisioned.**


Can we build machines that actively exploit the fundamental properties of quantum mechanics, such as the superposition principle or the existence of entangled states? Applications such as the transistor or the laser, often quoted as developments based on quantum mechanics, do not actually answer this question. Quantum mechanics enters into these devices only at the level of material properties, but their state variables such as voltages and currents remain classical. Proposals for true quantum machines emerged in the last decades of the 20th century and are now being actively explored: quantum computers (*1*), quantum cryptography communication systems (*2*), and detectors operating below the standard quantum limit (*3*). The major difficulty facing the engineer of a quantum machine is decoherence (*4*). If a degree of freedom needs to be manipulated externally, as in the writing of information, its quantum coherence usually becomes very fragile. Although schemes that actively fight decoherence have recently been proposed (*5*, *6*), they need very coherent quantum systems to start with. The quality of coherence for a two-level system can be quantitatively described by the quality factor of quantum coherence $Q_\varphi = \pi\nu_{01}T_\varphi$, where $\nu_{01}$ is its transition frequency and $T_\varphi$ is the coherence time of a superposition of the states. It is generally accepted that for active decoherence compensation mechanisms, $Q_\varphi$'s larger than $10^4\ \nu_{01}\ t_{op}$ are necessary, $t_{op}$ being the duration of an elementary operation (*7*).

Among all the practical realizations of quantum machines, those involving integrated electrical circuits are particularly attractive. However, unlike the electric dipoles of isolated atoms or ions, the state variables of a circuit, like voltages and currents, usually undergo rapid quantum decoherence because they are strongly coupled to an environment with a large number of uncontrolled degrees of freedom (*8*). Nevertheless, superconducting tunnel junction circuits (*9*–*13*) have displayed $Q_\varphi$'s up to several hundred (*14*), and temporal coherent evolution of the quantum state has been observed on the nanosecond time scale (*10*, *15*) in the case of the single Cooper pair box (*16*). We report here a new circuit built around the Cooper pair box with $Q_\varphi$ in excess of $10^4$, whose main feature is the separation of the write and readout ports (*17*, *18*). This circuit, which behaves as a tunable artificial atom, has been nicknamed a "quantronium."

The basic Cooper pair box consists of a low-capacitance superconducting electrode, the "island," connected to a superconducting reservoir by a Josephson tunnel junction with capacitance $C_j$ and Josephson energy $E_J$. The junction is biased by a voltage source $U$ in series with a gate capacitance $C_g$. In addition to $E_J$, the box has a second energy scale, the Cooper pair Coulomb energy $E_{CP} = (2e)^2/2(C_g + C_j)$ . When the temperature $T$ and the superconducting gap $\Delta$ satisfy $k_BT \ll \Delta/\ln N$ and $E_{CP} \ll \Delta$, where N is the total number of paired electrons in the island, the number of excess electrons is even (*19*, *20*). The Hamiltonian of the box is then

$$\hat{H} = E_{CP}(\hat{N} - N_g)^2 - E_J\cos\hat{\theta} \qquad (1)$$

where $N_g = C_gU/2e$ is the dimensionless gate


Quantronics Group, Service de Physique de l'Etat Condensé, Direction des Sciences de la Matière, Commissariat à l'Energie Atomique–Saclay, 91191 Gif-sur-Yvette, France.

*To whom correspondence should be addressed. E-mail: vion@drecam.saclay.cea.fr

†Member of CNRS.

‡Present address: Applied Physics Department, Yale University, New Haven, CT 06520, USA.

charge and $\hat{\theta}$ the phase of the superconducting order parameter in the island, conjugate to the number $\hat{N}$ of excess Cooper pairs in it (*16*).

In our experiment, $E_J \cong E_{CP}$ and neither $\hat{N}$ nor $\hat{\theta}$ is a good quantum number. The box thus has discrete quantum states that are quantum superpositions of several charge states with different $N$. Because the system is sufficiently nonharmonic, the ground $|0\rangle$ and first excited $|1\rangle$ energy eigenstates form a two-level system. This system corresponds to an effective spin one-half $\vec{s}$, whose Zeeman energy $h\nu_{01}$ goes to a minimal value close to $E_J$ when $N_g = 1/2$. At this particular bias point, both states $|0\rangle$ ($s_z = +1/2$) and $|1\rangle$ ($s_z = -1/2$) have the same average charge $\langle\hat{N}\rangle = 1/2$, and consequently the system is immune to first-order fluctuations of the gate charge. Manipulation of the quantum state is performed by applying microwave pulses $u(t)$ with frequency $\nu \cong \nu_{01}$ to the gate, and any superposition $|\Psi\rangle = \alpha\,|0\rangle + \beta\,|1\rangle$ can be prepared.

A novel type of readout has been implemented in this work. The single junction of the basic Cooper pair box has been split into two nominally identical junctions in order to form a superconducting loop (Fig. 1). The Josephson energy $E_J$ in Eq. 1 becomes $E_J \cos(\hat{\delta}/2)$ (*21*), where $\hat{\delta}$ is an additional degree of freedom: the superconducting phase difference across the series combination of the two junctions (*22*). The two states are discriminated not through the charge $\langle\hat{N}\rangle$ on the island (*10*, *23*), but through the supercurrent in the loop $\langle\hat{I}\rangle = (2e/\hbar)\langle\partial H/\partial\delta\rangle$. This is achieved by entangling $\vec{s}$ with the phase $\hat{\gamma}$ of a large Josephson junction with Josephson energy $E_{J0} \approx 20\,E_J$ inserted in the loop (*17*, *24*). The phases are related by $\hat{\delta} = \hat{\gamma} + \phi$, where $\phi = 2e\Phi/\hbar$, $\Phi$ being the external flux imposed through the loop. The junction is shunted by a capacitor $C$ to reduce phase fluctuations. A trapezoidal readout pulse $I_b(t)$, with a peak value slightly below the critical current $I_0 = 2eE_{J0}/\hbar$, is applied to the parallel combination of the large junction and the small junctions (Fig. 1C). When starting from $\langle\hat{\delta}\rangle \approx 0$, the phases $\langle\hat{\gamma}\rangle$ and $\langle\hat{\delta}\rangle$ grow during the current pulse, and consequently an $\vec{s}$-dependent supercurrent develops in the loop. This current adds to the bias current in the large junction, and by precisely adjusting the amplitude and duration of the $I_b(t)$ pulse, the large junction switches during the pulse to a finite voltage state with a large probability $p_1$ for state $|1\rangle$ and with a small probability $p_0$ for state $|0\rangle$ (*17*). This readout scheme is similar to the spin readout of Ag atoms in a Stern and Gerlach apparatus, in which the spin is entangled with the atom position. For the parameters of the experiment, the efficiency of this projective measurement should be $\eta = p_1 - p_0 = 0.95$ for optimum readout conditions. The readout is also designed so as to minimize the $|1\rangle \rightarrow |0\rangle$ relaxation rate using a Wheatstone bridge–like symmetry. Large ratios $E_{J0}/E_J$ and $C/C_j$ provide further protection from the environment. Just as the system is immune to charge noise at $N_g = 1/2$, it is immune to flux and bias current noise at $\phi = 0$ and $I_b = 0$, where $\hat{I} = 0$. The preparation of the quantum state and its manipulation are therefore performed at this optimal working point.

A quantronium sample is shown in Fig. 1B. It was fabricated with standard e-beam lithography and aluminum evaporation. The sample was cooled down to 15 mK in a dilution refrigerator. The switching of the large junction (*25*) to the finite voltage state is detected by measuring the voltage across it with a room-temperature preamplifier, followed by a discriminator. By repeating the experiment, the switching probability, and hence the occupation probabilities of the $|0\rangle$ and $|1\rangle$ states, can be determined.

The readout part of the circuit was tested by measuring the switching probability $p$ at thermal equilibrium as a function of the pulse height $I_p$, for a readout pulse duration of $\tau_R = 100$ ns. The discrimination between the estimated currents for the $|0\rangle$ and $|1\rangle$ states was found to have an efficiency of $\eta = 0.6$, which is lower than the expected $\eta = 0.95$. Measurements of the switching probability as a function of temperature and repetition rate indicate that the discrepancy between the theoretical and experimental readout efficiency could be due to an incomplete thermalization of our last filtering stage in the bias current line.

Spectroscopic measurements of $\nu_{01}$ were performed by applying to the gate a weak continuous microwave irradiation suppressed just before the readout pulse. The variations of the switching probability as a function of the irradiation frequency display a resonance whose center frequency evolves with dc gate voltage and flux as the Hamiltonian predicts, reaching $\nu_{01} \cong 16.5$ GHz at the optimal working point (Fig. 2). The small discrepancy

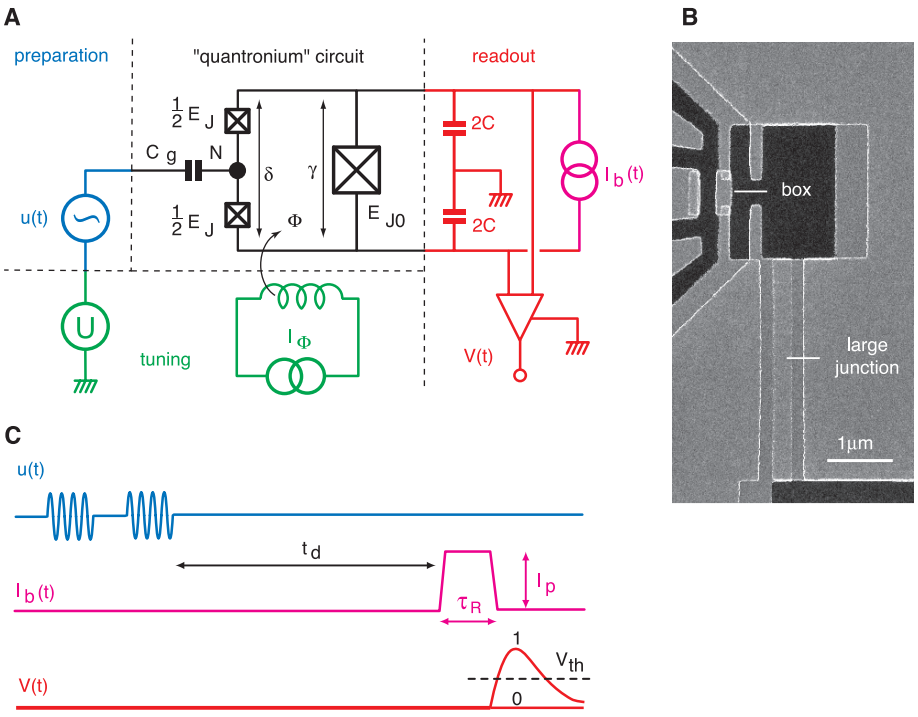


**Fig. 1.** (**A**) Idealized circuit diagram of the quantronium, a quantum-coherent circuit with its tuning, preparation, and readout blocks. The circuit consists of a Cooper pair box island (black node) delimited by two small Josephson junctions (crossed boxes) in a superconducting loop. The loop also includes a third, much larger Josephson junction shunted by a capacitance $C$. The Josephson energies of the box and the large junction are $E_J$ and $E_{J0}$. The Cooper pair number $N$ and the phases $\delta$ and $\gamma$ are the degrees of freedom of the circuit. A dc voltage $U$ applied to the gate capacitance $C_g$ and a dc current $I_\Phi$ applied to a coil producing a flux $\Phi$ in the circuit loop tune the quantum energy levels. Microwave pulses $u(t)$ applied to the gate prepare arbitrary quantum states of the circuit. The states are read out by applying a current pulse $I_b(t)$ to the large junction and by monitoring the voltage $V(t)$ across it. (**B**) Scanning electron micrograph of a sample. (**C**) Signals involved in quantum state manipulation and measurement. Top: Microwave voltage pulses $u(t)$ are applied to the gate for state manipulation. Middle: A readout current pulse $I_b(t)$ with amplitude $I_p$ is applied to the large junction $t_d$ after the last microwave pulse. Bottom: Voltage $V(t)$ across the junction. The occurrence of a pulse depends on the occupation probabilities of the energy eigenstates. A discriminator with threshold $V_{th}$ converts $V(t)$ into a boolean output for statistical analysis.

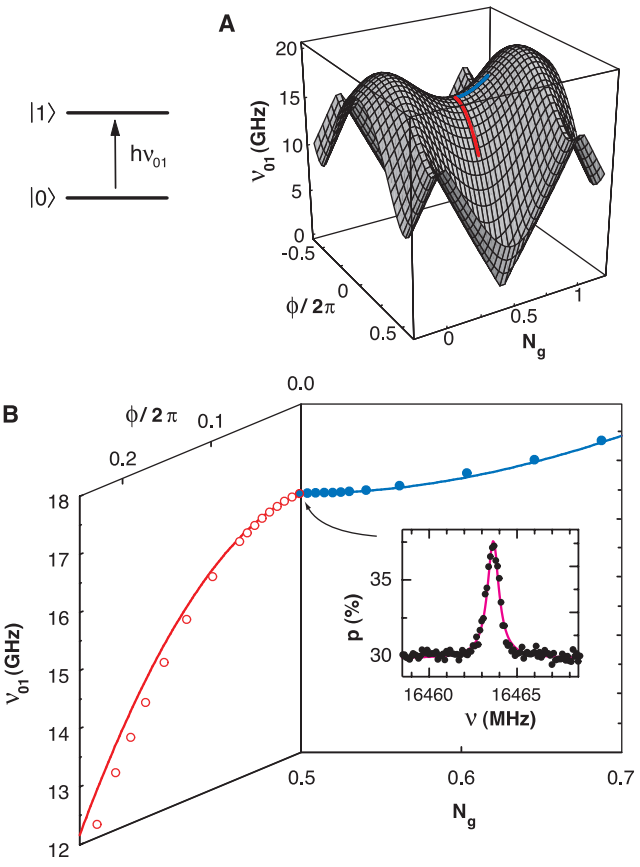


**Fig. 2.** (**A**) Calculated transition frequency $\nu_{01}$ as a function of $\phi$ and $N_g$ for $E_J = 0.865\ k_BK$ and $E_J/E_{CP} = 1.27$. The saddle point at the intersection of the blue and red lines is an ideal working point where the transition frequency is independent, to first order, of the bias parameters. (**B**) Measured center transition frequency (symbols) as a function of reduced gate charge $N_g$ for reduced flux $\phi = 0$ [right panel, blue line in (A)] and as a function of $\phi$ for $N_g = 0.5$ [left panel, red line in (A)], at 15 mK. Spectroscopy is performed by measuring the switching probability $p$ ($10^5$ events) when a continuous microwave irradiation of variable frequency is applied to the gate before readout ($t_d < 100$ ns). Continuous line: Theoretical best fit leading to $E_J$ and $E_J/E_{CP}$ values indicated above. Inset: Lineshape measured at the optimal working point $\phi = 0$ and $N_g = 0.5$ (dots). Lorentzian fit with a FWHM $\Delta\nu_{01} = 0.8$ MHz and a center frequency $\nu_{01} = 16463.5$ MHz (solid line).

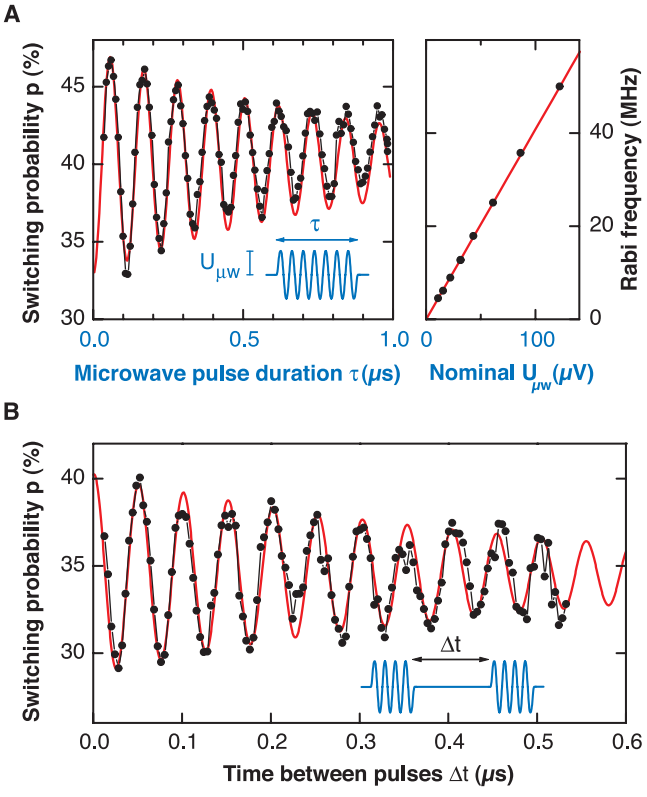


**Fig. 3.** (**A**) Left: Rabi oscillations of the switching probability $p$ ($5 \times 10^4$ events) measured just after a resonant microwave pulse of duration $\tau$. Data were taken at 15 mK for a nominal pulse amplitude $U_{\mu w} = 22\ \mu V$ (joined dots). The Rabi frequency is extracted from an exponentially damped sinusoidal fit (continuous line). Right: Measured Rabi frequency (dots) varies linearly with $U_{\mu w}$, as expected. (**B**) Ramsey fringes of the switching probability $p$ ($5 \times 10^4$ events) after two phase-coherent microwave pulses separated by $\Delta t$. Joined dots: Data at 15 mK; the total acquisition time was 5 mn. Continuous line: Fit by exponentially damped sinusoid with time constant $T_\phi = 0.50\ \mu s$. The oscillation corresponds to the beating of the free evolution of the spin with the external microwave field. Its period indeed coincides with the inverse of the detuning frequency (here $\nu - \nu_{01} = 20.6$ MHz).

between theoretical and experimental values of the transition frequency at nonzero magnetic flux is attributed to flux penetration in the small junctions not taken into account in the model. These spectroscopic data have been used to precisely determine the relevant circuit parameters, $E_J = 0.865\ k_BK$ and $E_J/E_{CP} = 1.27$. At the optimal working point, the linewidth was found to be minimal, with a 0.8-MHz full width at half-maximum (FWHM). When varying the delay between the end of the irradiation and the readout pulse, the resonance peak height decays with a time constant $T_1 = 1.8\ \mu s$. Supposing that the energy relaxation of the system is only due to the bias circuitry, a calculation similar to that in (*26*) predicts that $T_1 \sim 10\ \mu s$ for a crude discrete element model. This result shows that no detrimental sources of dissipation have been seriously overlooked in our circuit design.

Controlled rotations of $\vec{s}$ around an axis $x$ perpendicular to the quantization axis $z$ have been performed. Before readout, a single pulse at the transition frequency with variable amplitude $U_{\mu w}$ and duration $\tau$ was applied. The resulting change in switching probability is an oscillatory function of the product $U_{\mu w}\tau$ (Fig. 3A), which is in agreement with the theory of Rabi oscillations (*27*), proving that the resonance indeed arises from a two-level system. The proportionality ratio between the Rabi period and $U_{\mu w}\tau$ was used to calibrate microwave pulses for the application of controlled rotations of $\vec{s}$.

Rabi oscillations correspond to a driven coherent evolution but do not give direct access to the intrinsic coherence time $T_\varphi$ during a free evolution of $\vec{s}$. This $T_\varphi$ was obtained by performing a Ramsey fringe experiment (*28*), on which atomic clocks are based. One applies to the gate two phase-coherent microwave pulses, each corresponding to a $\pi/2$ rotation around $x$ (*29*) and separated by a delay $\Delta t$, during which the spin precesses freely around $z$. For a given detuning of the microwave frequency, the observed decaying oscillations of the switching probability as a function of $\Delta t$ (Fig. 3B) correspond to the "beating" of the spin precession with the external microwave field (*30*). The oscillation period agrees exactly with the inverse of the detuning, allowing a measurement of the transition frequency with a relative accuracy of $6 \times 10^{-6}$. The envelope of the oscillations yields the decoherence time $T_\varphi \cong 0.50\ \mu s$. Given the transition period $1/\nu_{01} \cong 60$ ps, this means that $\vec{s}$ can perform on average 8000 coherent free precession turns.

In all the time domain experiments on the quantronium, the oscillation period of the switching probability agrees closely with theory, which proves controlled manipulation of $\vec{s}$. However, the amplitude of the oscillations is smaller than expected by a factor of 3 to 4.

This loss of contrast is likely to be due to a relaxation of the level population during the measurement itself.

In order to understand what limits the coherence time of the circuit, measurements of the linewidth $\Delta\nu_{01}$ of the resonant peak as a function of $U$ and $\Phi$ have been performed. The linewidth increases linearly when departing from the optimal point ($N_g = 1/2$, $\phi = 0$, $I_b = 0$). This dependence is well accounted for by charge and phase noises with root mean square deviations $\Delta N_g = 0.004$ and $\Delta(\delta/2\pi) = 0.002$ during the time needed to record the resonance. The residual linewidth at the optimal working point is well explained by the second-order contribution of these noises. The amplitude of the charge noise is in agreement with measurements of $1/f$ charge noise (*31*), and its effect could be minimized by increasing the $E_J/E_{CP}$ ratio. The amplitude of the flux noise is unusually large (*32*) and should be significantly reduced by improved magnetic shielding. An improvement of $Q_\varphi$ by an order of magnitude thus seems possible. Experiments on quantum gates based on the controlled entanglement of several capacitively coupled quantronium circuits could already be performed with the level of quantum coherence achieved in the present experiment.

**References and Notes**


1. M. A. Nielsen, I. L. Chuang, *Quantum Computation and Quantum Information* (Cambridge Univ. Press, Cambridge, 2000).
2. *The Physics of Quantum Information: Quantum Cryptography, Quantum Teleportation, Quantum Computation*, D. Bouwmeester, A. Ekert, A. Zeilinger, Eds. (Springer-Verlag, Berlin, 2000).
3. V. B. Braginsky, F. Ya. Khalili, *Quantum Measurement* (Cambridge Univ. Press, 1992).
4. W. H. Zurek, J. P. Paz, in *Coherent Atomic Matter Waves*, R. Kaiser, C. Westbrook, F. David, Eds. (Springer-Verlag, Heidelberg, Germany, 2000).
5. P. W. Shor, *Phys. Rev. A* **52**, R2493 (1995).
6. A. M. Steane, *Phys. Rev. Lett.* **77**, 793 (1996); *Rep. Prog. Phys.* **61**, 117 (1998).
7. J. Preskill, *J. Proc. R. Soc. London Ser.* A **454**, 385 (1998)
8. Y. Makhlin, G. Schön, A. Shnirman, *Rev. Mod. Phys.* **73**, 357 (2001).
9. M. H. Devoret *et al.*, in *Quantum Tunneling in Condensed Media*, Y. Kagan, A. J. Leggett, Eds. (Elsevier Science, Amsterdam, 1992).
10. Y. Nakamura, Yu. A. Pashkin, J. S. Tsai, *Nature* **398**, 786, (1999).
11. C. H. van der Wal *et al.*, *Science* **290**, 773 (2000).
12. S. Han, R. Rouse, J. E. Lukens, *Phys. Rev. Lett.* **84**, 1300 (2000).
13. S. Han, Y. Yu, X. Chu, S. -I. Chu, Z. Wang, *Science* **293**, 1457 (2001).
14. J. M. Martinis, S. Nan, J. Aumentado, and C. Urbina (unpublished data) have recently obtained $Q_\varphi$'s reaching 1000 for a current-biased Josephson junction.
15. Y. Nakamura, Yu. A. Pashkin, T. Yamamoto, J. S. Tsai, *Phys. Rev. Lett.* **88**, 047901 (2002).
16. V. Bouchiat, D. Vion, P. Joyez, D. Esteve, M. H. Devoret, *Phys. Scr.* **T76**, 165 (1998).
17. A. Cottet *et al.*, *Physica C* **367**, 197 (2002).
18. Another two-port design has been proposed by A. B. Zorin [*Physica C* **368**, 284 (2002)].
19. M. T. Tuominen, J. M. Hergenrother, T. S. Tighe, M. Tinkham, *Phys. Rev. Lett.* **69**, 1997 (1992).
20. P. Lafarge, P. Joyez, D. Esteve, C. Urbina, M. H. Devoret, *Nature* **365**, 422 (1993).
21. D. V. Averin, K. K. Likharev, in *Mesoscopic Phenomena in Solids*, B. L. Altshuler, P. A. Lee, R. A. Webb, Eds. (Elsevier, Amsterdam, 1991).
22. J. R. Friedman, D. V. Averin, *Phys. Rev. Lett.* **88**, 50403 (2002).
23. A. Aassime, G. Johansson, G. Wendin, R. J. Schoelkopf, P. Delsing, *Phys. Rev. Lett.* **86**, 3376 (2001).
24. A different Cooper pair box readout scheme using a large Josephson junction is discussed by F. W. J. Hekking, O. Buisson, F. Balestro, and M. G. Vergniory, in *Electronic Correlations: From Meso- to Nanophysics*, T. Martin, G. Montambaux, J. Trân Thanh Vân, Eds. (Editions De Physique, Les Ulis, France, 2001), pp. 515–520.
25. For $C = 1$ pF and $I_0 = 0.77$ μA, the bare plasma frequency of the large junction is $\omega_p/2\pi \cong 8$ GHz, well below $\nu_{01}$.
26. A. Cottet *et al.*, in *Macroscopic Quantum Coherence and Quantum Computing*, D. V. Averin, B. Ruggiero, P. Silvestrini, Eds. (Kluwer Academic, Plenum, New York, 2001), pp. 111–125.
27. I. I. Rabi, *Phys. Rev.* **51**, 652 (1937).
28. N. F. Ramsey, *Phys. Rev.* **78**, 695 (1950).
29. In practice, the rotation axis does not need to be $x$, but the rotation angle of the two pulses is always adjusted so as to bring a spin initially along $z$ into the plane perpendicular to $z$.
30. At fixed $\Delta t$, the switching probability displays a decaying oscillation as a function of detuning.
31. H. Wolf *et al.*, *IEEE Trans. Instrum. Meas.* **46**, 303 (1997).
32. F. C. Wellstood, C. Urbina, J. Clarke, *Appl. Phys. Lett.* **50**, 772 (1987).



33. The indispensable technical work of P. Orfila is gratefully acknowledged. This work has greatly benefited from direct inputs from J. M. Martinis and Y. Nakamura. The authors acknowledge discussions with P. Delsing, G. Falci, D. Haviland, H. Mooij, R. Schoelkopf, G. Schön, and G. Wendin. Partly supported by the European Union through contract IST-10673 SQUBIT and the Conseil Général de l'Essone through the EQUM project.

26 December 2001; accepted 20 March 2002


# Coherent Temporal Oscillations of Macroscopic Quantum States in a Josephson Junction


**Yang Yu,[1] Siyuan Han,[1]* Xi Chu,[2]† Shih-I Chu,[2] Zhen Wang[3]**



**We report the generation and observation of coherent temporal oscillations between the macroscopic quantum states of a Josephson tunnel junction by applying microwaves with frequencies close to the level separation. Coherent temporal oscillations of excited state populations were observed by monitoring the junction's tunneling probability as a function of time. From the data, the lower limit of phase decoherence time was estimated to be about 5 microseconds.**


The question of whether macroscopic variables obey quantum mechanics has stimulated extensive theoretical interests (*1*, *2*). The experimental search for macroscopic quantum phenomena (MQP) did not start until the early 1980s, when theory showed that the experimental conditions for observing MQP in Josephson junction–based devices were achievable (*3*–*5*). Many MQP, such as macroscopic quantum tunneling (MQT) (*6*–*10*), energy level quantization (*11*, *12*), quantum incoherent relaxation (*13*), resonant tunneling and photon-assisted tunneling (*14*), and photo-induced transition and population inversion between macroscopic quantum states (*15*, *16*), have since been observed. Recent spectroscopy evidence of superposition of fluxoid states and persistent-current states in superconducting quantum interference devices has also been reported (*17*, *18*). However, time domain coherent oscillations between macroscopic quantum states (MQS), which is more direct evidence for the superposition of MQS, has thus far evaded experimental detection.

One of the methods proposed to create coherent temporal oscillations between two MQS is via Rabi oscillation, an effect that is well established and understood in atomic and molecular systems (*19*). The principle of Rabi oscillations is that by applying a monochromatic electromagnetic (EM) field to a quantum two-level system, which interacts with the EM fields, the system will be in a superposition of the two energy eigenstates that results in oscillations between the lower and upper levels with Rabi frequency $\Omega$. The amplitude of the population oscillations is at a maximum when the frequency of the EM wave $\omega$ is in resonance with the level spacing $\Delta E$, i.e., $\omega = \Delta E/\hbar$. Rabi oscillation is a coherent quantum phenomenon that provides the foundation to a wide variety of basic research and applications, ranging from coherent excitation of atoms and molecules by laser to quantum computation (*20*–*22*). Re-


[1]Department of Physics and Astronomy, [2]Department of Chemistry, University of Kansas, Lawrence, KS 66045, USA. [3]Kansai Advanced Research Center, Communication Research Laboratory, Ministry of Posts and Telecommunications, 588-2 Iwaoka, Iwaoka-cho, Nishi-ku, Kobe, 651-24 Japan.

*To whom correspondence and requests should be addressed. E-mail: han@ku.edu

†Present address: Institute for Theoretical Atomic and Molecular Physics, Harvard-Smithsonian Center for Astrophysics, 60 Garden Street, Cambridge, MA 02138, USA.